Progress In Electromagnetics Research, PIER 75, 357–381, 2007

A NEW RAY-TRACING BASED WAVE PROPAGATION MODEL INCLUDING ROUGH SURFACES SCATTERING

Y. Cocheril and R. Vauzelle

SIC Lab., Université de Poitiers
Bât. SP2MI, Téléport 2, Blvd Marie et Pierre Curie
BP 30179, 86962 Futuroscope Chasseneuil Cedex, France

Abstract—This paper presents a complete ray-tracing based model which takes into account scattering from rough surfaces in indoor environments. The proposed model relies on a combination between computer graphics and radar techniques. The paths between the transmitter and the receiver are found thanks to a Bi-Directional Path-Tracing algorithm, and the scattering field after each interaction between the electromagnetic wave and the environment is computed according to the Kirchhoff Approximation. This propagation model is implemented as a plug-in in an existing full 3-D ray-tracing software. Thus, we compare the results of classical ray-tracing with those of our model to study the influence of the scattering phenomenon on the wave propagation in typical indoor environments.

1. INTRODUCTION

Millimetric systems, which supply wide band applications like wireless local area networks, are currently attracting a lot of interest. The carrier frequencies of these systems increase up to 10 GHz to transmit multimedia information in indoor environments like full high definition videos. In order to deploy such high bit rate wireless systems, the study of radio channel behaviour is necessary depending on specific wave propagation conditions.

There are many methods for studying radio channels. In respect of the millimetric waves studied in this paper, numerical and rigorous methods like FDTD, MoM or Integral Methods are not suitable. Because of the environment and wavelength dimensions, these methods involve an overlong computational time. Another one could rest

onto hybridization between several different schemes like FDTD, Finite Volume (FVTD) and Time Integrated Methods (TIM) [1]. Nevertheless, none of them are suitable in regard of the overall cost (in terms of memory and CPU time) to perform the computation of a large scene [2–5]. The main restrictive point to these approaches lies into the necessity to mesh the free space between the obstacles/sources.

A better choice is to use asymptotic techniques in these environments which give a good performance/accuracy ratio. These methods compute all the possible paths followed by the electromagnetic (EM) wave between a transmitter and a receiver in a given environment. In particular, ray-tracing (RT) techniques [6] are fast and applicable as long as the wavelength is smaller than the dimensions of objects encountered during the propagation of an EM wave. Thanks to Geometric Optics (GO) [7] and its extensions, the Geometrical/Uniform Theory of Diffraction (GTD/UTD) [8, 9], RT respectively takes into account reflection / transmission and diffraction phenomena. The scattering effects of an EM wave from rough surfaces are usually discarded in RT because the scattering phenomenon could be ignored with the present system frequencies.

The scattering of an EM wave can be classified in two components according to the level roughness of the surface we consider [10] (1). When the roughness is smaller than the wavelength, the scattering phenomenon is equivalent to specular reflection from a smooth surface. In this case, the reflected wave follows classical Snell's law and its magnitude is computed using the classical Fresnel reflection coefficients. When the roughness level increases the diffuse component appears. The energy contained in the specular direction is distributed in others around it. One popular guideline for characterising the surface roughness is the Rayleigh criterion [10], which states that a surface is smooth if:

$$\sigma_h < \frac{\lambda}{8\,\cos\left(\theta_{inc}\right)} \tag{1}$$

where σ_h represents the standard deviation of the heights, θ_{inc} is the incident angle between the EM wave and the normal to the surface, and λ is the carrier wavelength.

Many techniques exist for including rough surface scattering in RT models. One such technique modifies the Fresnel reflection coefficient with an attenuation factor according to the roughness level, only in the specular direction [11, 12]. Thus, the roughness Fresnel reflection coefficient in both polarisations (parallel // and perpendicular $\perp$) is expressed as:

$$R^m_{//,\perp} = \rho_s\, R_{//,\perp} \tag{2}$$

where $R_{//,\perp}$ is the classical Fresnel reflection coefficient, and $\rho_s \in [0, 1]$

is the attenuation factor, usually equal to:

$$\rho_s = \exp\left[-8\left(\frac{\pi\,\sigma_h\,\cos\left(\theta_{inc}\right)}{\lambda}\right)^2\right] \tag{3}$$

The main drawback of the attenuation factor is that it gives only the scattering field in the specular direction and not in numerous other ones around it.

A second solution consists in using an empirical scattering function [13] which gives the scattering field according to the roughness level and the difference in angle between the specular component and the angle to the receiver. The major drawback of this technique comes from its empirical formulation which limits its use to some specific indoor environments and wave propagation conditions.

Thirdly, a hybrid solution based on ray-tracing and radiance techniques is proposed in [14]. Based on an Oren model [15] to compute the diffuse component, this model uses a V-cavity roughness model, so it is limited to Gaussian slope distributions. Approximations have also been made to simplify its complex formulation.

In this paper we present a complete RT based model which takes into account scattering from rough surfaces overcoming the previous drawbacks [16]. Indeed, our model computes the scattering field in all possible directions and it does not depend on a specific environment. Moreover, it allows Gaussian and not Gaussian rough surfaces to be taken into account. Briefly, our model is a combination of computer graphics and radar techniques. A Bi-Directional Path-Tracing (BDPT) algorithm [17] is used to compute the paths the EM wave follows between the transmitter and the receiver, and the scattering field after each interaction between the EM wave and the environment is computed according to the Kirchhoff Approximation (KA) [10, 18].

This paper is structured as follows: after introducing our KA based scattering model in Section 2, we explain how it can take Gaussian or not rough surfaces in Section 3. In Section 4, the BDPT algorithm is presented in detail. In Section 5, the proposed method is applied to some examples and compared with classical 3-D ray-tracing to show the scattering influence on the EM wave propagation.

2. MICRO–FACET BASED SCATTERING MODEL

Firstly, we present the model used to compute the scattering field from a rough surface, before treating a full wave propagation in a 3-D indoor environment. The following model is based on the well known Kirchhoff Approximation (KA) [10, 18]. So the rough surface

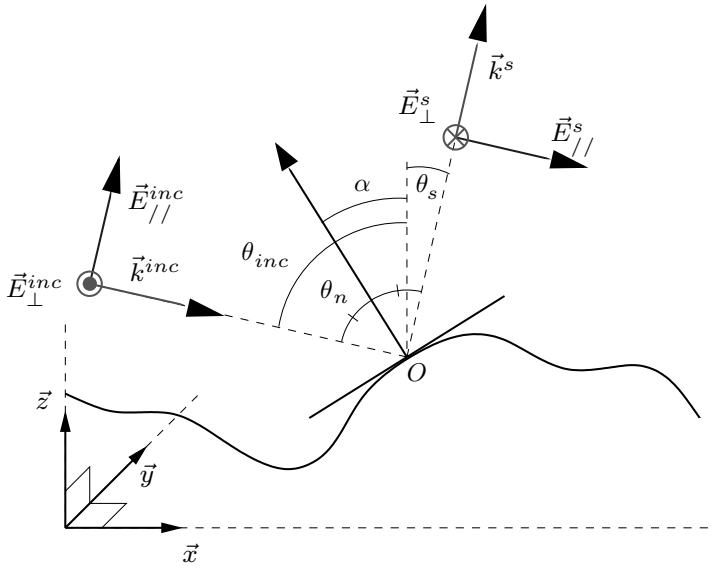

Figure 1. Notations used in the KA based scattering model apply to a rough profile oriented in $\vec{x}$ direction.

is decomposed into micro-facets, i.e., into small planes that are locally tangent to the roughness. Fig. 1 represents a rough profile, an arbitrary tangent plane on it, and the notations used hereafter for the incident and the scattered fields.

2.1. Scattering Field by a Single Micro-facet

The decomposed rough profile is illuminated with an incident plane wave. Thus, each micro-facet receives the same part of the incident plane wave and reflects it in its own specular direction. As in the smooth surface case, this particular direction is defined by the incident angle θ_{inc} and the orientation of the local normal α of a micro-facet. Hence, the scattering field can be computed as in the smooth surface case and it can be written for a specific micro-facet:

$$\vec{E}^s_{//,\perp} = R_{//,\perp}(\theta_{inc}, \theta_s)\ \vec{E}^{inc}_{//,\perp}\ e^{-j\varphi}\ e^{-j(\phi_{inc}+\phi_s)} \tag{4}$$

where $\vec{E}^s_{//,\perp}$ and $\vec{E}^{inc}_{//,\perp}$ are the scattered and the incident fields respectively in both polarisations, $R_{//,\perp}(\theta_{inc}, \theta_s)$ is the local Fresnel reflection coefficient between the incident θ_{inc} and the scattered θ_s directions, and $e^{-j(\phi_{inc}+\phi_s)}$ is the phase shifting due to the free space

propagation distance before, ϕ_{inc}, and after, ϕ_s, the interaction. The term $e^{-j\varphi}$ corresponding to the phase shifting due to the height h of the local micro-facet with respect to the global mean value which is usually set at $h = 0$. It is directly linked to the Rayleigh criterion (1) and can be written:

$$\varphi = \frac{4\,\pi}{\lambda}\, h\, \cos\left(\theta_{inc}\right) \tag{5}$$

2.2. Scattering Field by All Micro-facets of a Rough Profile

In this context, we have to make a coherent sum of all the contributions of the scattered fields encapsulated in a small solid angle $d\theta$ around a specific direction θ_s, in order to take into account interferences due to the possible various heights of the corresponding micro-facets. Indeed, many micro-facets can be oriented in the same direction but they are not automatically at the same height, depending on the global mean value. If n micro-facets among a total number N are well directed, the coherent sum is equal to a vector sum per component ($\vec{x}$, $\vec{y}$, $\vec{z}$) of the scattered fields:

$$\vec{E}^{s}_{//,\perp} = \sum_{i=1}^{n}\ \vec{E}^{s}_{//,\perp,i} \tag{6}$$

where $\vec{E}^{s}_{//,\perp,i}$ is the scattering field in both polarisations of the i^{th} micro-facet (4).

Because of the plane wave propagation condition, the scattering field for the i^{th} micro-facet can be simplified as follows:

$$\vec{E}^{s}_{//,\perp,i} = R_{//,\perp,i}\left(\theta_{inc},\theta_s\right)\ e^{-j\varphi_i}\ \vec{E}^{inc}_{//,\perp,i}\ \underbrace{e^{-j(\phi_{inc}+\phi_s)}}_{=\,C^{te}} \tag{7}$$

Now, we are going to express the total scattering field around a specific direction, for the parallel component. Note that the same reasoning can be applied out for the perpendicular polarisation. So, in parallel polarisation, the scattering field of the i^{th} micro-facet among N can be decomposed as:

$$\vec{E}^{s}_{//,i}\left(\theta_s\right) = \begin{cases} R_{//}(\theta_{inc},\,\theta_s)\ \dfrac{1}{N}\ \cos\left(\theta_s\right)\ e^{-j\varphi_i}\ C^{te}\ \vec{x} \\ 0\ \vec{y} \\ R_{//}(\theta_{inc},\,\theta_s)\ \dfrac{1}{N}\ \sin\left(\theta_s\right)\ e^{-j\varphi_i}\ C^{te}\ \vec{z} \end{cases} \tag{8}$$

Then, the vector sum of n contributions contained in $d\theta$ around

θ_s direction is equal to:

$$\vec{E}^s_{//}(\theta_s) = \begin{cases} C^{te}\ R_{//}(\theta_{inc},\theta_s)\dfrac{1}{N}\cos(\theta_s)\displaystyle\sum_{i=1}^{n}\left\{e^{-j\varphi_i}\right\}\vec{x} \\ 0\ \vec{y} \\ C^{te}\ R_{//}(\theta_{inc},\theta_s)\dfrac{1}{N}\sin(\theta_s)\displaystyle\sum_{i=1}^{n}\left\{e^{-j\varphi_i}\right\}\vec{z} \end{cases} \tag{9}$$

If we introduce the ratio $\frac{n}{n}$ in (9), the scattering field into a solid angle $d\theta$ around the direction θ_s as becomes:

$$|\vec{E}^s_{//}(\theta_s)| = R_{//}(\theta_{inc},\,\theta_s)\ C^{te}\ \frac{n}{N}\ \frac{1}{n}\ \sum_{i=1}^{n} e^{-j\varphi_i} \tag{10}$$

where $\frac{n}{N}$ represents the probability of having n well directed micro-facets in θ_s direction among N possible, and $\frac{1}{n}\sum_{i=1}^{n} e^{-j\varphi_i}$ corresponds to the mean attenuation due to the phase shifting connected to the heights of well directed micro-facets.

The scattering field in θ_s direction can be written according to the probability density function $p(\theta_s)$, to have a well directed micro-facet around a specific direction:

$$|\vec{E}^s_{//}(\theta_s)| = R_{//}(\theta_{inc},\,\theta_s)\ C^{te}\ p(\theta_s)\ \frac{1}{n}\ \sum_{i=1}^{n} e^{-j\varphi_i} \tag{11}$$

We can deduce from (11) the scattering coefficient $\sigma^{//,\perp}(\theta_s)$ in both polarisations, which gives the ratio between the scattered power in a solid angle $d\theta$ around θ_s and the incident power:

$$\sigma^{//,\perp}(\theta_s) = |\vec{E}^s_{//,\perp}(\theta_s)|\ |\vec{E}^s_{//,\perp}(\theta_s)|^* \tag{12}$$

3. GAUSSIAN AND NON-GAUSSIAN ROUGH SURFACES

We have seen in the previous section that the scattering field in a specific direction θ_s depends on the probability density function (PDF) $p(\theta_s)$ to have a well directed micro-facet. This section shows how it can be possible to compute the scattering field on various kind of rough surfaces, thanks to this parameter.

In this paper, we separate rough surfaces into two different categories, 1) continuous rough surfaces, and 2) non-continuous rough surfaces, depending on whether they have a continuous PDF or not. In the first case, the PDF $p(\theta_s)$ can be modelled by a theoretical law, while in the second case we have to tabulate it.

3.1. Continuous Rough Surfaces

In this category, we can distinguish two cases, Gaussian and non-Gaussian rough surfaces.

3.1.1. Gaussian Rough Surfaces

Usually rough surfaces are considered Gaussian, i.e., they have a Gaussian distribution of the heights and their autocorrelation function is Gaussian too. This assumption can be expressed as follows:

$$p_h(h) = \frac{1}{\sqrt{2\,\pi}\,\sigma_h}\, e^{-\frac{1}{2}\left(\frac{h}{\sigma_h}\right)^2} \tag{13}$$

and

$$R_h(l) = e^{-\left(\frac{l}{L_c}\right)^2} \tag{14}$$

where $p_h(h)$ is the Gaussian PDF of the heights, $R_h(l)$ is the autocorrelation function which gives the correlation between two heights separated by a distance l, and L_c is the correlation length obtained for $R_h(L_c) = \frac{1}{e}$.

In this particular case, we can link the PDF $p_h(\theta_s)$ to the main parameters of the two previous functions, 1) the standard deviation of the heights σ_h and 2) the correlation length L_c. Indeed, the PDF $p_h(h')$ of the slopes h' is also Gaussian [10, 19]:

$$p_h(h') = \frac{1}{\sqrt{2\,\pi}\,\sigma_{h'}}\, e^{-\frac{1}{2}\left(\frac{h'}{\sigma_{h'}}\right)^2} \tag{15}$$

where the standard deviation of the slopes is $\sigma_{h'} = \sqrt{2}\ \frac{\sigma_h}{L_c}$.

According to the relation

$$h' = \tan(\alpha) \tag{16}$$

and using the change of variables

$$p(a)\,|da| = p(b)\,|db| \tag{17}$$

we can express from (15) the PDF $p_h(\alpha)$ of the local normals α:

$$p_h(\alpha) = \frac{L_c}{2\,\sqrt{\pi}\,\sigma_h\,\cos^2(\alpha)}\ e^{-\left(\frac{\tan(\alpha)\,L_c}{2\,\sigma_h}\right)^2} \tag{18}$$

Then, in the case of a mono-dimensional rough profile, there is a simple relationship between the local normals and the scattering directions θ_s, according to the incident angle θ_{inc}:

$$\alpha = \frac{\theta_s + \theta_{inc}}{2} \tag{19}$$

Hence, we can deduce from (18) and (19) the PDF $p_h(\theta_s)$ of the scattering directions:

$$p_h(\theta_s) = \frac{L_c}{4\sqrt{\pi}\,\sigma_h\,\cos^2(\alpha)}\; e^{-\left(\frac{\tan(\alpha)\,L_c}{2\,\sigma_h}\right)^2} \tag{20}$$

In the case of 1D rough surfaces, the scattering field (11) can be computed replacing the $p(\theta_s)$ coefficient with the relationship (20). In the case of 2D rough surfaces, it does not exist a simple relationship that links the local normals orientation and the scattering direction. A simple solution is to compute the orientations of all the micro-facets of a rough surface according to two orthogonal directions $\vec{x}$ and $\vec{y}$. These two variables are supposed independent, so the PDF $p_h(\theta_s) = p_h(\theta_s)_{\vec{x}}\; p_h(\theta_s)_{\vec{y}}$ is the joint probability to have simultaneously a good orientation in the both $\vec{x}$ and $\vec{y}$ directions. This method allows to treat 2D rough surfaces, whether they are isotropic or not.

3.1.2. Non-Gaussian Rough Surfaces

We have seen previously that if a rough surface is Gaussian, its slope distribution is Gaussian too and depends on the height standard deviation and the correlation length. Now, if a rough surface is not Gaussian, the link between the height and the slope distributions does not exist. So it is easier to characterise directly the slopes or the local normals distributions rather than the heights distribution and the autocorrelation function.

In this case, we can use a great number of theoretical laws to model the slopes or the local normals according to the rough surfaces we want to use. In this study we are particularly interested in a decomposition of a Gaussian law in Hermite polynomials [20]. It involves an asymptotic expansion of the Gaussian distribution [21]. This latter is multiplied by polynomials corresponding to the successive terms in Edgeworth series. These terms have a direct relationship with central moments, so we can include the skewness γ_3 (21) and the kurtosis γ_4 (22) in addition to the mean and the standard deviation.

$$\gamma_3 \quad = \quad \frac{\mu_3}{\sigma^3} \tag{21}$$

$$\gamma_4 \quad = \quad \frac{\mu_4}{\sigma^4} \tag{22}$$

where μ_i is the i^{th} central moment.

In the following, the formalism is expressed for the slopes h'. So, let the standard Gaussian distribution be:

$$\varphi_{h'}(f) = \frac{1}{\sqrt{2\pi}\sigma_{h'}}\, e^{-\frac{f^2}{2}} \tag{23}$$

with $f = \frac{h'-m_{h'}}{\sigma_{h'}}$.

The asymptotic expression of the Gaussian distribution can be expressed at different orders $O \in \{2,3,4\}$ in terms of the central moments which are taken into account:

$$p_{h'}(h') = \varphi_{h'}(f)\ \psi_{h'}(f) \tag{24}$$

where

$$\psi_{h'}(f) = \begin{cases} 1, & O=2 \\ 1+\dfrac{\gamma_{3_{h'}}}{6}H_3(f), & O=3 \\ 1+\dfrac{\gamma_{3_{h'}}}{6}H_3(f)+\dfrac{\gamma_{4_{h'}}-3}{24}H_4(f)+\dfrac{\gamma_{3_{h'}}^2}{72}H_6(f), & O=4 \end{cases} \tag{25}$$

with

$$H_3(f) \quad = \quad f^3-3f \tag{26}$$

$$H_4(f) \quad = \quad f^4-6f^2+3 \tag{27}$$

$$H_6(f) \quad = \quad f^6-15f^4+45f^2-15 \tag{28}$$

Using (16), (19) and (24), the PDF $p_{h'}(\theta_s)$ can be expressed as:

$$p_{h'}(\theta_s) = \frac{1}{2\cos^2(\alpha)}\ \varphi_{h'}(f_{h'})\ \psi_{h'}(f_{h'}) \tag{29}$$

where

$$f_{h'} = \frac{\tan\left(\dfrac{\theta_s+\theta_{inc}}{2}\right)-m_{h'}}{\sigma_{h'}} \tag{30}$$

The same reasoning can be followed using the local normals modelling as a starting point. In this case, the PDF $p_\alpha(\theta_s)$ can be expressed as:

$$p_\alpha(\theta_s) = \frac{1}{2}\ \varphi_\alpha(f_\alpha)\ \psi_\alpha(f_\alpha) \tag{31}$$

where

$$f_\alpha = \frac{\frac{\theta_s + \theta_{inc}}{2} - m_\alpha}{\sigma_\alpha} \tag{32}$$

3.1.3. Application on Three Real Rough Surfaces of Indoor Roughcasts

To give an example, a previous study [22] has compared the modelling results between deterministic and statistical distributions of the heights, the slopes and the local normals of three samples of real rough surfaces of indoor roughcasts (Fig. 2), using the Kolmogorov-Smirnov criterion [23]. These three roughcasts are named R1, R2 and R3 according to an increasing roughness level and an increasing similarity between their deterministic height distributions and a Gaussian law. It has been shown that it is better to use the local normals including high order moments like the skewness and the kurtosis to model the studied rough surfaces.

In this paper, we continue our investigations, studying the influence of the PDF $p_{h,h',\alpha}(\theta_s)$ on the scattering field computation

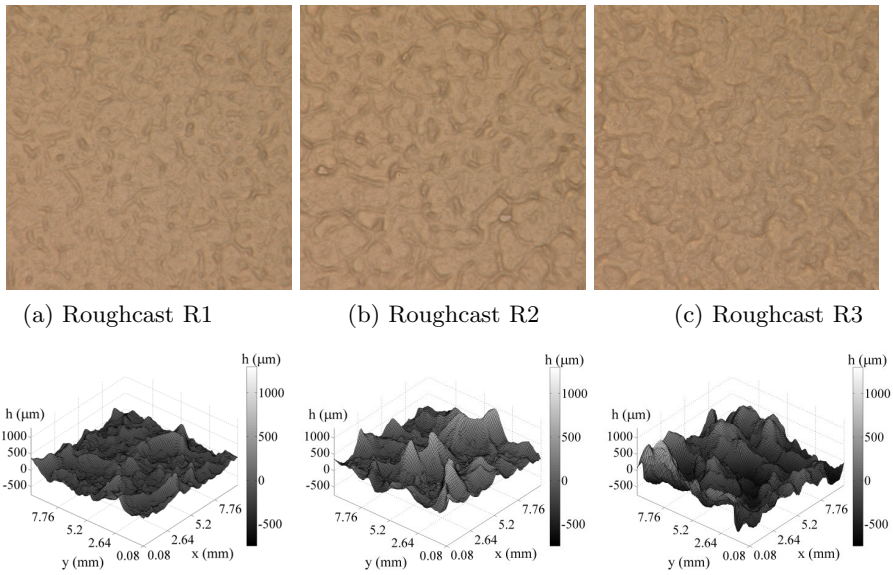

(a) Roughcast R1 (b) Roughcast R2 (c) Roughcast R3

(c) Heights map of R1 (d) Heights map of R2 (e) Heights map of R3

Figure 2. Images and heights maps of three real indoor roughcasts, sorted in an increasing level of roughness.

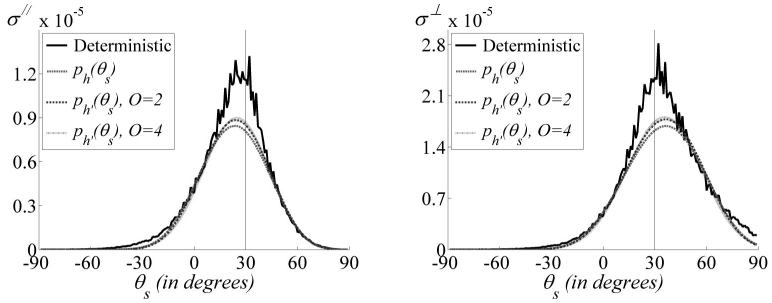

(a) parallel polarisation (b) perpendicular polarisation

Figure 3. Scattering coefficients computation using the slopes (profile in $\vec{x}$ direction from R1).

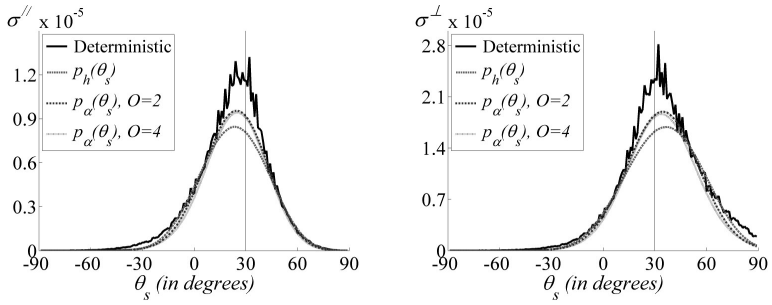

(a) parallel polarisation (b) perpendicular polarisation

Figure 4. Scattering coefficients computation using the local normals (profile in $\vec{x}$ direction from R1).

(11). The three surfaces of roughcast are illuminated with a plane wave, with a unit power, an incident $\theta_{inc} = 30°$ and a wavelength $\lambda = 0.005\,\mathrm{m}$ ($f = 60\,\mathrm{GHz}$). Figs. 3 and 4 show the scattering coefficients in both polarisations (//, $\perp$) using the slopes h' or the local normals α to find the PDF $p(\theta_s)$. In each figure, the scattering coefficients obtained using the PDF $p_{h,h',\alpha}(\theta_s)$ are compared with the scattering coefficients computed using the deterministic rough surface or making a Gaussian hypothesis on the heights. In the deterministic case, all the micro-facets of a real rough surface sample receive the same quantity of energy and we compute the scattering field from all of them using (7). Thus, the real orientations and phase shifting due to the heights of the micro-facets are taken into account. To complete our observations, we compare in Table 1 the mean square errors (MSE) between all the statistical scattering coefficients and the deterministic

Table 1. MSE results between scattering coefficients computed with the deterministic and the statistical distributions.

	R1		R2		R3	
Direction	x	y	x	y	x	y
Model	$MSE_{\sigma//}$ $(.10^{-7})$					
$p_h(\theta_s)$	11.57	15.08	7.85	5.14	4.20	3.70
$p_{h'}(\theta_s),\ O=2$	11.51	12.86	10.12	10.25	7.16	6.42
$p_{h'}(\theta_s),\ O=4$	11.23	12.11	9.79	9.31	7.51	6.67
$p_\alpha(\theta_s),\ O=2$	8.74	9.27	4.40	9.20	10.81	4.55
$p_\alpha(\theta_s),\ O=4$	8.05	12.88	4.83	9.64	11.16	4.75
Model	$MSE_{\sigma^\perp}$ $(.10^{-7})$					
$p_h(\theta_s)$	23.27	29.64	19.62	11.66	8.31	9.81
$p_{h'}(\theta_s),\ O=2$	23.08	25.45	21.54	22.21	14.23	15.67
$p_{h'}(\theta_s),\ O=4$	22.45	23.87	22.35	21.05	15.10	17.14
$p_\alpha(\theta_s),\ O=2$	19.35	19.81	11.61	18.57	23.42	14.38
$p_\alpha(\theta_s),\ O=4$	18.27	27.24	14.01	19.26	22.91	14.79

ones.

Figs. 3 and 4 show that the statistical scattering coefficients computed for the roughcast R1 in the $\vec{x}$ direction are closer than the deterministic ones if we use PDF $p_\alpha(\theta_s)$. The skewness and the kurtosis do not have a really significant influence on these results, but they do have a major effect on the modelling of the rough surface parameters [22]. So, in this case, it is better to use the local normals to compute the scattering coefficients than the slopes or the heights.

These observations are confirmed by the MSE results. Table 1 shows that the error between the deterministic and the statistical scattering coefficients is minimised when we use, 1) the local normals when the surface is far from Gaussian like R1, and 2) the heights when the surface is quietly Gaussian as R2 and R3.

3.2. Non-continuous Rough Surfaces

The second category of rough surfaces is composed of surfaces which do not have a continuous PDF of their own parameters. For example, building facades can be considered rougher in outdoor (Fig. 5(a)) than in indoor environments for lower frequency systems like WiMAX or LMDS. This example shows, for a profile of a specific facade, that the height variations (Fig. 5(b)) and the corresponding PDF of the local normals (Fig. 5(c)) do not have continuous values.

Deduced from the PDF $p_\alpha(\alpha)$ using (19), the PDF $p_\alpha(\theta_s)$ can

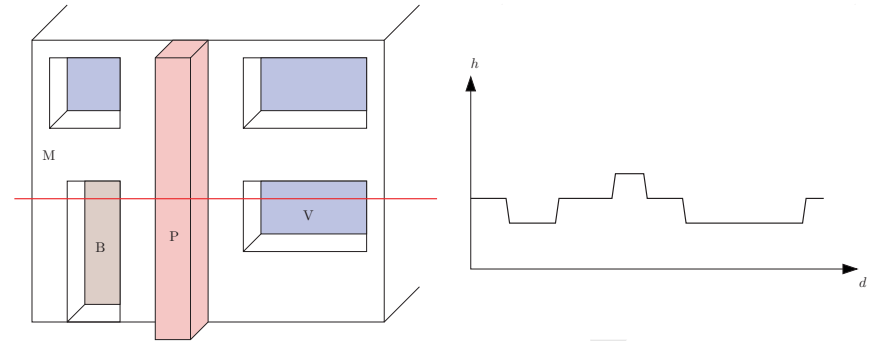

(a) Facade of a building (b) Height variations of a profile

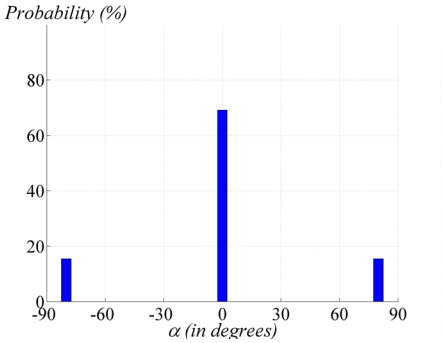

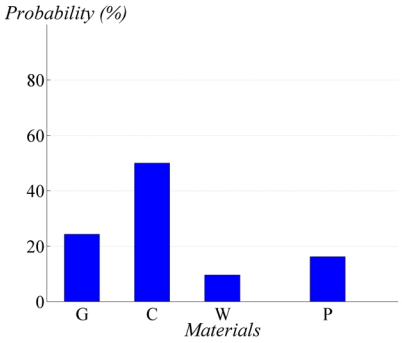

(c) PDF of the local normals $p_\alpha(\alpha)$ (d) PDF of the corresponding materials

Figure 5. Decomposition of a building facade according to the height variations – (W) wood, (G) glass, (C) concrete, (P) plastic.

not be modelled using classical theoretical laws. So it is tabulated, i.e., the possible scattering directions are stored in a table with the corresponding probabilities of having a well directed micro-facet. When the scattering model is used, we compute the scattering field for each possible direction θ_s.

Moreover, the non-continuous rough surfaces are not composed of a single material. We can compute the global PDF of the materials (Fig. 5(d)) for the present example. In reality, we have one PDF of the materials for each orientation α. So, when we choose an orientation we know the probability of having a specific material.

This original description of complex real surfaces, associated to the scattering model proposed in Section 2, contributes to a simple modelling of the environment and allows the computation of the corresponding scattering coefficient. Indeed, each surface is

represented by a flat polygon and characterised by its corresponding PDF (orientations and materials). However, in a preliminary step, it will be necessary to evaluate all the PDF of the surfaces which make up the environment.

4. BI-DIRECTIONAL PATH-TRACING ALGORITHM

This section presents an algorithm which includes the scattering phenomenon in a full 3D wave propagation simulation in an environment made up of many rough surfaces.

We have been inspired by the research work carried out in the computer graphics field since the nineteen-sixties to solve the global illumination problem. This work has led to many algorithms [24–28, 17] based on Monte-Carlo methods [29]. Briefly, their goal is to compute the light intensity received using RT techniques. In this area of research, the transmitters are the light sources and the receivers are the pixels of an image of the simulated environment. The main principle consists in propagating the light rays from the light sources in the environment. When a light ray interacts with an object, the intensity of the reflected light is computed according to a scattering model defined in the visible domain.

This principle is greatly similar to our problem, the propagation of an electromagnetic wave using GO. Indeed, we have only to replace the transmitters and the receivers by antennas, and the scattering computation of the light intensity by the scattering model presented in Section 2. Taking into account the polarized nature of the electromagnetic waves, computer graphics algorithms will be applied to the propagation of the electromagnetic waves.

Firstly, this section presents the adaptation of the formalism in the computer graphics field to electromagnetic wave propagation. Then we present the algorithm deduced from it to simulate electromagnetic wave propagation in a real environment including the scattering model seen in Section 2.

4.1. Adaptation of Computer Graphics Techniques to Our Problem

4.1.1. The Rendering Equation

The rendering equation (33) is a formulation of the global illumination problem [25]. This equation expresses the interactions which occur during the light propagation in a given environment. In the visible domain, this equation expresses the received luminance at the point x and re-emitted in the direction θ_s, according to the received luminance

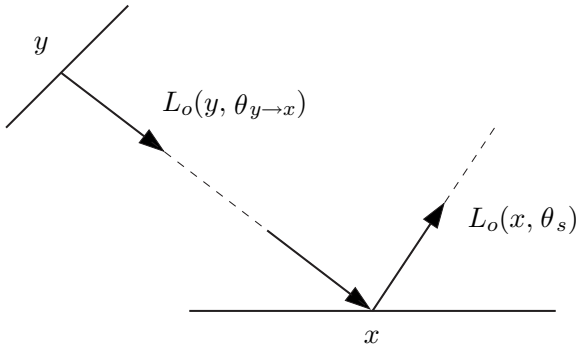

Figure 6. Definition of the variables used in the rendering equation formalism.

in x from other objects in the environment (Fig. 6). The rendering equation is thus:

$$L_o(x,\theta_s) = L_e(x,\theta_s) + \int_A \left\{ f_r(x,\theta_{y\to x},\theta_s)\, L_o(y,\theta_{y\to x}) \right. \\ \left. V(x,y)\, \frac{\cos(\theta_{y\to x})\, \cos(\theta_s)}{s^2(x,y)}\, dy \right\} \tag{33}$$

where

- A is the integral domain, i.e. all the surfaces of the environment,
- $L_e(x,\theta_s)$ is the self luminance of the point x, assuming it is a light source,
- $L_o(y,\theta_{y\to x})$ is the luminance emitted from the point y toward the point x, noted $\theta_{y\to x}$,
- $f_r(x,\theta_{y\to x},\theta_s)$ is the Bi-directional Reflectance Distribution Function (BRDF). It expresses the ratio of the incident power at the point x from the direction $\theta_{y\to x}$, which is reflected in the direction θ_s. It can be expressed as:

$$f_r(x,\theta_{inc},\theta_s) = \frac{\partial L_o(x,\theta_s)}{L_{inc}(x,\theta_{inc})\, \cos(\theta_n)\, \partial\omega_{inc}} \tag{34}$$

- $V(x,y)$ is a visibility function between x and y,
- dy is a differential surface around the point y.

4.1.2. Adaptation to Electromagnetic Wave Propagation

We have to express the equivalent to the rendering equation with electromagnetic terms. In electromagnetism, we do not compute the received luminance, but the received electromagnetic field. Moreover, (33) can be simplified: the term $L_e(x, \theta_s) = 0$ because a surface of an object in the environment will not be a transmitter. Hence, the rendering equation in electromagnetism can be written:

$$\vec{E}^s_{//,\perp}(x, \theta_s) = \int_A \left\{ f_r^{EM}(x, \theta_{y\to x}, \theta_r)\, \vec{E}^s_{//,\perp}(y, \theta_{y\to x}) \right. \\ \left. e^{-jks(y,x)}\, V(x, y)\, dy \right\} \tag{35}$$

where $\theta_{y\to x}$ is equivalent to θ_{inc}, $e^{-jks(y,x)}$ is the attenuation due to the free space propagation between the points x and y, separated by a distance $s(x, y)$, and k is the wave number. Note that the use of electromagnetic values simplifies the term $[\cos(\theta_{y\to x})\, \cos(\theta_s)]/s^2(x, y)$.

The equivalent to the BRDF in electromagnetism, f_r^{EM}, is given by the scattering model we proposed in Section 2 (11). In this case, it expresses the ratio between the reflected power and the incident power at the point x on a surface of the environment, according to a specific incident polarisation and to a specific combination of the angles (θ_{inc}, θ_s). It can be expressed from (11) as:

$$f_r^{EM}(x, \theta_{inc}, \theta_s) = R_{//,\perp}(\theta_{inc},\, \theta_s)\, p(\theta_{inc},\, \theta_s)\, \frac{1}{n} \sum_{i=1}^{n} e^{-j\varphi_i} \tag{36}$$

Thanks to the Monte-Carlo methods which transform an infinite integral to a finite one:

$$\begin{aligned} I &= \int_\Omega f(x)\, dx = \int_\Omega \frac{f(x)}{p(x)}\, p(x)\, dx = \int_\Omega g(x)\, p(x)\, dx \\ &\simeq \frac{1}{n} \sum_{1}^{n} g(x) \end{aligned} \tag{37}$$

the electromagnetic BRDF $f_r^{EM}(x, \theta_{inc}, \theta_s)$ becomes:

$$\begin{aligned} f_r^{EM}(x, \theta_{inc}, \theta_s) &= R_{//,\perp}(\theta_{inc},\, \theta_s)\, p(\theta_{inc}, \theta_s) \\ &\quad \int_\Omega e^{-j\varphi(h, \theta_{inc}, \theta_s)}\, p(h)\, dh \end{aligned} \tag{38}$$

The equivalent to the rendering equation in electromagnetism is applied to all combinations of points (x, y) generating an extensive

integral equations system which controls the field, or energy exchanges between the objects in the environment. We chose to use the BDPT algorithm to solve these integral equations presented in the next section.

4.2. BDPT Algorithm

The BDPT [17] is a Monte-Carlo based algorithm to solve the rendering equation. It consists in combining two Path-Tracing algorithms to improve the quality and the accuracy of the results [30].

4.2.1. Unidirectional Path-Tracing (PT)

Its main principle [25] is to emit and to propagate a great number of rays from the receiver in an environment, and to compute the contribution of those which pass through the transmitter (solid lines in Fig. 7(a)). The main drawback of this technique is that the probability of having a path which passes precisely through the transmitter is close to 0.

The solution is to use the next event estimation [31] which consists in separating the recursive integral in the rendering equation into two other ones. The first one is computed to a given point while the second is recursive from this point. In practice, this principle is expressed by the direct illumination computation: we send a ray from the transmitter to each interaction point (dashed lines in Fig. 7(a)) found during the propagation of the path emitted from the receiver.

While the next event estimation improves the Path-Tracing, this method is unusable in complex environments. When there are many obstacles between the receiver and the transmitter, the probability of having an existing path between these two points is actually close to 0. The BDPT algorithm provides a solution to this problem.

4.2.2. Bi-Directional Path-Tracing (BDPT)

Bi-directional Path-Tracing (BDPT) involves the clever combination of two PT in order to improve the probability of finding paths between the receiver and the transmitter. They are led simultaneously and independently, the first one from the receiver and the second one from the transmitter.

The main principle is to launch one ray from the receiver and another from the transmitter and to propagate them in the environment (solid lines in Fig. 7(b)), according to a maximum number of interactions. Then, we check whether a Line Of Sight (LOS) exists between each combination of two interaction points $S_i S'_j \ \forall i, j \in [1, 3]$

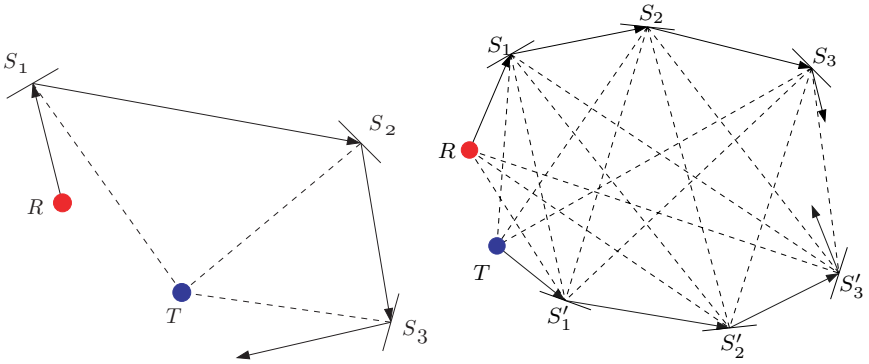

(a) Path-Tracing (b) Bi-Directional Path-Tracing

Figure 7. Path-Tracing and bi-directional Path-Tracing main principles.

(dashed lines in Fig. 7(b)). In the positive case, a part of the power can pass from a path to the other one, depending on the scattering model applied at each interaction point. Thus a path between the receiver and the transmitter can probability exist.

Finally, the BDPT algorithm (Fig. 8) is implemented in an existing full 3D ray-tracing software, CRT (Communication Ray Tracer) [32], using a plug-in. It allows the simulation and characterization of the radio channel in various environments computing the wide band channel parameters, such as mean delay, delay spread, ...

5. CHANNEL SIMULATIONS

In this section, we study the influence of the scattering phenomenon on the radio link computing the impulse responses and the corresponding delay spreads in several indoor environments at millimetric frequencies. To do this, we use the scattering model seen in Section 2, the rough surfaces described in Section 3 and the BDPT algorithm proposed in Section 4 to simulate wave propagation. The rough surfaces are made up of plaster:

$$\begin{aligned} \mu &= 1\ H.m^{-1} \\ \varepsilon &= 6\ F.m^{-1} \\ \sigma &= 0.1\ S.m^{-1} \end{aligned}$$

We carry out the study in three different environments with an increasing level of complexity (Fig. 9), in terms of the minimum

Require: 3D modelled environment: material and rough properties of each object, antennas positions T and R, ...
Require: Maximum number of interactions N_I
Require: Maximum number of launched rays N_R
for $i = 0$ to N_R **do**
  Initialisation of the i^{th} random path from T : T^i_{path}
  $k \leftarrow 1$
  while (intersection(T^i_{path},object) = **true**) **AND** ($k \leq N_I$) **do**
    $Q^k_T \leftarrow k^{th}$ interaction point on T^i_{path}
    $I^k_T \leftarrow$ rough informations in Q^k_T
    if (visibility(Q^k_T,R) = **true**) **then**
      Computation of the probability to have a reflected ray from $Q^k_T \rightarrow R$, according to I^k_T
      Computation of the received field magnitude in R
    end if
    Choice of a reflected direction from Q^k_T, according to I^k_T
    Update of T^i_{path}
    $k \leftarrow k + 1$
  end while
  Initialisation of the i^{th} random path from R : R^i_{path}
  $j \leftarrow 1$
  while (intersection(R^i_{path},object) = **true**) **AND** ($j \leq N_I$) **do**
    $Q^j_R \leftarrow j^{th}$ interaction point on R^i_{path}
    $I^j_R \leftarrow$ rough informations in Q^j_R
    for $k = 1$ to N_I **do**
      if (visibility(Q^j_R,Q^k_T) = **true**) **AND** ($j + k \leq N_I$) **then**
        Computation of the probability to have a reflected ray from $Q^j_R \rightarrow Q^k_E$, according to I^j_R
        Computation of the received field magnitude in R from the path $\{E \dots Q^{k-1}_E \; Q^k_E \; Q^j_R \; Q^{j-1}_R \dots R\}$
      end if
    end for
    Choice of a reflected direction from Q^j_R, according to I^j_R
    Update of R^i_{path}
    $j \leftarrow j + 1$
  end while
  $i \leftarrow i + 1$
end for

Figure 8. Bi-directional Path-Tracing algorithm.

interaction number required to reach the receiver from the transmitter. Each environment is successively composed of R1, R2 and R3 rough surfaces. Note that a simulation using a classical RT is also performed for each environment, assuming the surfaces are smooth. All the simulations are computed using $N_I = 10$ interactions.

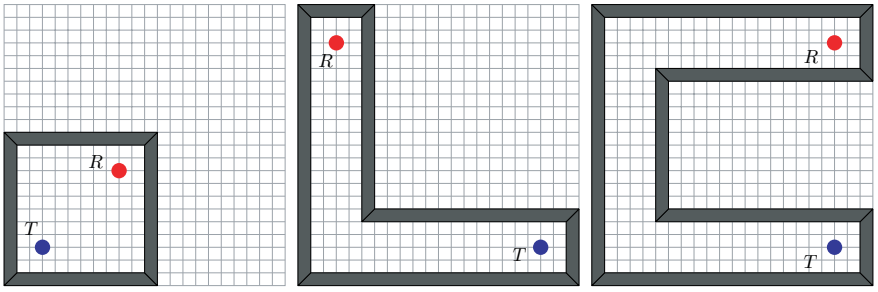

(a) cubic room (b) L-shaped corridor (c) U-shaped corridor

Figure 9. Three tested indoor environments (10 m × 10 m).

5.1. Cubic Environment

The impulse responses (IRs) simulated in the cubic environment are plotted in Fig. 10(a). The first observation is the difference between the results obtained without (RT) and with roughness (R1, R2, R3). This difference is due to the dispersion of the energy around the specular reflection induced by the scattering phenomenon.

To illustrate this principle, we plot in Fig. 10(b) only RT and R1 impulse responses (IRs), obtained for only two interactions. In the smooth surfaces case, a single path is found, of about $\tau = 30$ ns, while with the scattering phenomenon, the attenuation is greater, associated with the creation of new paths just before and after this delay value. The energy which disappears is re-distributed in new paths.

Then, for a delay $\tau < 10$ ns, we can see that some paths have a smaller attenuation using the scattering phenomenon than using the classical reflection on smooth surfaces. This phenomenon is linked to the previous principle. Indeed, these paths are close, so that when the energy of one is scattered in new ones, constructive and destructive interferences occur in the neighbouring paths, varying their attenuation.

Finally, it may be noted that the magnitude of the first path does not evolve whether or not rough surface scattering is used. Indeed, this specific path is the direct path, so it does not interact with the environment.

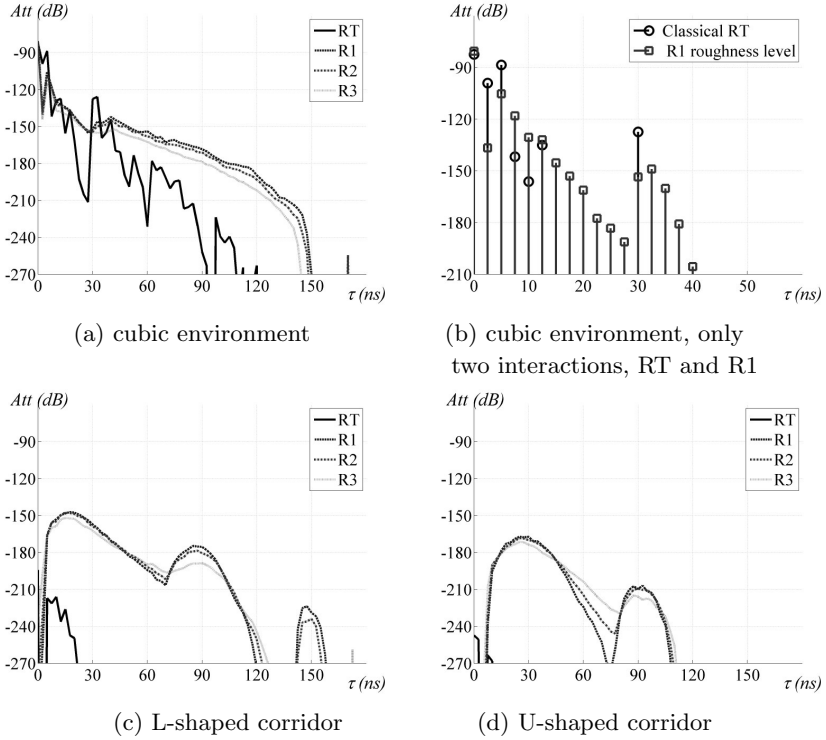

(a) cubic environment

(b) cubic environment, only two interactions, RT and R1

(c) L-shaped corridor

(d) U-shaped corridor

Figure 10. Impulse response (IR) results in the three tested environments with, and without roughness.

In the case of 10 interactions, it is more difficult to observe this principle and to analyse the plotted curves in Fig. 10(a). The interferences between scattering paths have the effect of decreasing the main paths found in the smooth surface case with RT, and of increasing those which were not significant. IRs are smoothed when the roughness level increases. The direct consequence for the channel parameter is a reduction of the delay spread when the roughness level increases.

5.2. Environment with a L Form

In this specific environment, the IRs Fig. 10(c) have a different behaviour depending on whether or not the roughness is taken into account. In the smooth surface case, a minimum of $N_I = 7$ interactions is required to have at least a received ray, so that few paths are found with a high attenuation.

If we take into account the scattering phenomenon by means of the BDPT algorithm, the probability of reaching the receiver increases due to the dispersion of the energy around the specular direction. Thus some paths are found for only $N_I = 1$ interaction. Globally, the received paths have suffered a lower number of interactions, so they have a smaller attenuation than the paths computed with the RT.

As in the cubic environment, the increase of the roughness leads to a general diminution of the attenuation of the main paths with a smoothing of the IRs. In other words, the dispersion of the energy around the specular direction increases with the roughness level.

5.3. Environment with a U Form

Fig. 10(d) presents the IRs results obtained in environment with a U form. The probability of receiving a path decreases in this environment in comparison with the previous environment (L). Indeed, a minimum of $N_I = 9$ interactions is necessary, so the paths found using RT are very few, and greatly attenuated. As in the L form, the scattering phenomenon increases the probability of having a received ray. For the similar reasons, the contributions of these rays are significant on the IRs. In a same way, the smoothing of the IRs increases when the roughness level also increases.

6. CONCLUSION

This paper has presented a complete model to include rough surface scattering in an electromagnetic wave propagation simulation.

Based on the Kirchhoff Approximation to compute the scattering field from a surface (Section 2), our formulation of the problem enables different kinds of rough surfaces to be taken into account. They can be Gaussian, non-Gaussian, characterised by a probability density function, or they can have a non-continuous distribution of the orientation of their micro-facets (Section 3). In this last case, one solution consists in tabulating the possible orientations. This approach is very interesting, because we can take into account all the surfaces usually discarded in indoor or outdoor environments, like building facades. A short study has shown that the scattering model leads to results substantially in accordance with deterministic ones, when we choose an appropriate theoretical law.

In Section 4, we present the main principle of our model and the corresponding algorithm used to simulate electromagnetic wave propagation in a given environment. Inspired by computer graphics techniques used to solve the global illumination problem, the bi-

directional Path-Tracing algorithm has been adapted to our problem and implemented in a Ray-Tracing software in a plugin form.

The first application has been presented in Section 5. It consists in simulating three indoor environments composed of the studied rough surfaces described in Section 3. In comparison with classical ray-tracing results (smooth surfaces), the scattering phenomenon smoothed the impulse responses by a spreading of energy over time due to the creation of new paths.

In the future, we will need to carry out a validation campaign of the proposed model, using measurements in real environments or rigorous methods like Integral Equations.

ACKNOWLEDGMENT

The authors would like to thank Christophe BOURLIER for its advices and background in Electromagnetic and scattering fields, and Philippe BLASI and Lilian AVENEAU for their help and support in Image Computing field, making this work possible.

REFERENCES

1. Breto, R. and A. Monorchio, "Time-domain hybrid methods to solve complex electromagnetic problems," EMC Congress, Istambul, 2003.
2. Maystre, D., "Electromagnetic scattering by a set of objects: an integral method based on scattering operator," *Progress In Electromagnetics Research*, PIER 57, 55–84, 2006.
3. Al Sharkawy, M. H., V. Demir, and A. Z. Elsherbeni, "The iterative multi-region algorithm using a hybrid finite difference frequency domain and method of moment techniques," *Progress In Electromagnetics Research*, PIER 57, 19–32, 2006.
4. Wang, S., X. Guan, D. Wang, X. Ma, and Y. Su, "Electromagnetic scattering by mixed conducting/dielectric objects using higher-order MoM," *Progress In Electromagnetics Research*, PIER 66, 51–63, 2006.
5. Mouysset, V., P. A. Mazet, and P. Borderies, "Efficient treatment of 3d time-domain electromagnetic scattering scenes by disjointing sub-domains and with consistent approximations," *Progress In Electromagnetics Research*, PIER 71, 41–57, 2007.
6. Deschamps, G. A., "Ray techniques in electromagnetics," *Proc. IEEE*, Vol. 60, No. 9, 1022–1035, September 1972.

7. Balanis, C. A., *Advanced Engineering Electromagnetics*, John Wiley and Sons, 1989.
8. Keller, J. B., "Geometrical theory of diffraction," *J. Opt. Soc. Am.*, Vol. 52, No. 2, 116–130, 1962.
9. Kouyoumjian, R. G. and P. H. Pathak, "A uniform geometrical theory of diffraction for an edge in a perfectly conducting surface," *Proc. IEEE*, Vol. 62, No. 11, 1448–1461, November 1974.
10. Beckmann, P. and A. Spizzichino, *The Scattering of Electromagnetic Waves from Rough Surfaces*, Pergamon, 1963.
11. Ament, W. S., "Toward a theory of reflection by a rough surface," *Proc. IEEE*, Vol. 41, No. 1, 142–146, January 1953.
12. Boithias, L., *Radio Wave Propagation*, McGraw-Hill, 1987.
13. Anderson, H. R., "A second generation 3-D ray-tracing model using rough surface scattering," *VTC '1996 Proceedings*, Vol. 1, 46–50, IEEE, Atlanta, USA, May 1996.
14. Ng, K. H., E. K. Tameh, and A. R. Nix, "A new hybrid geometrical optics and radiance based scattering model for ray-tracing applications," *ICC '2005 Proceedings*, Vol. 4, 2168–2172, IEEE, Seoul, Korea, May 2005.
15. Oren, M. and S. K. Nayar, "Generalization of the Lambertian model and implications for machine vision," *International Journal of Computer Vision*, Vol. 14, No. 3, 227–251, April 1995.
16. Didascalou, D., M. Dottling, N. Geng, and W. Wiesbeck, "An approach to include stochastic rough surface scattering into deterministic ray-optical wave propagation modeling," *IEEE Trans. Antennas Propagat.*, Vol. 51, No. 7, 1508–1515, July 2003.
17. Lafortune, E. P. and Y. D. Willems, "Bi-directional path tracing," *SIGGRAPH '1993 Proceedings*, 145–153, Computer Graphics, Alvor, Portugal, December 1993.
18. Ogilvy, J. A., *Theory of Wave Scattering from Random Rough Surfaces*, Institute of Physics Publishing, 1991.
19. Ulaby, F. T., R. K. Moore, and A. K. Fung, *Microwave Remote Sensing: Active and Passive*, Vol. II: Radar Remote Sensing and Surface Scattering and Emission Theory, Artech House, 1986.
20. Edgeworth, F. Y., *On the Representation of Statistical Frequency by a Series*, JRSS, 1907.
21. Longuet-Higgins, M. S., "The effect of non-linearities on statistical distributions in the theory of sea waves," *J. Fluid Mech.*, Vol. 17, 459–480, 1963.
22. Cocheril, Y., R. Vauzelle, and L. Aveneau, "3-D channel simulations including scattering from non-Gaussian rough surfaces,"

VTC '2006 Proceedings, 1–5, IEEE, Montreal, Canada, September 2006.

23. Chakravarti, I. M., R. G. Laha, and J. Roy, *Handbook of Methods of Applied Statistics*, Vol. 1, John Wiley and Sons, 1967.
24. Appel, A., "Some techniques for shading machine renderings of solids," *in AFIPS 1968 Spring Joint Computer Conf.*, Vol. 32, 37–45, 1968.
25. Kajiya, J. T., "The rendering equation," *Computer Graphics*, Vol. 20, No. 4, 143–150, August 1986.
26. Goral, C. M., K. E. Torrance, D. P. Greenberg, and B. Battaile, "Modelling the interaction of light between diffuse surfaces," *SIGGRAPH '84 Proceedings*, Vol. 18, 212–222, Computer Graphics, Minneapolis, USA, July 1984.
27. Whitted, T., "An improved illumination model for shaded display," *Communications of the ACM*, Vol. 23, No. 6, 343–349, 1980.
28. Jensen, H. W. and N. J. Christensen, "Photon maps in bi-directional Monte-Carlo Ray-Tracing of complex objects," *Computers and Graphics*, Vol. 19, No. 2, 215–224, March 1995.
29. Hammersley, J. M. and D. C. Handscomb, *Monte-Carlo Methods*, Chapman and Hall, 1964.
30. Cocheril, Y., S. Reynaud, and R. Vauzelle, "Comparison between two original methods including scattering in 3D channel simulations," *ECWT '2006 Proceedings*, IEEE, Manchester, England, September 2006.
31. Lafortune, E. P., "Mathematical models and Monte-Carlo algorithms for physically based rendering," Ph.D. Dissertation, Katholieke Universiteit Leuven, February, 1996.
32. Pousset, Y., R. Vauzelle, L. Aveneau, and M. Mériaux, "Characterization of the mobile channel by a 3-D UTD propagation model," *PSIP '2001*, Marseille, France, January 2001.